Biosensors and Bioelectronics (xxxx) xxxx–xxxx

Contents lists available at ScienceDirect

Biosensors and Bioelectronics

journal homepage: www.elsevier.com/locate/bios

Electrochemical H_2O_2 biosensor composed of myoglobin on MoS_2 nanoparticle-graphene oxide hybrid structure

Jinho Yoon[a], Taek Lee[a,b], Bharate Bapurao G.[a], Jinhee Jo[a], Byung-Keun Oh[a,*], Jeong-Woo Choi[a,b,*]

[a] Department of Chemical & Biomolecular Engineering, Sogang University, 35 Baekbeom-Ro, Mapo-Gu, Seoul 121-742, South Korea
[b] Institute of Integrated Biotechnology, Sogang University, 35 Baekbeom-Ro, Mapo-Gu, Seoul 121-742, South Korea

ARTICLE INFO

Keywords:
MoS_2 nanoparticle
Graphene oxide
Myoglobin
Biosensor
Hydrogen peroxide
Electrochemical signal enhancement

ABSTRACT

In this research, the electrochemical biosensor composed of myoglobin (Mb) on molybdenum disulfide nanoparticles (MoS_2 NP) encapsulated with graphene oxide (GO) was fabricated for the detection of hydrogen peroxide (H_2O_2). Hybrid structure composed of MoS_2 NP and GO (GO@MoS_2) was fabricated for the first time to enhance the electrochemical signal of the biosensor. As a sensing material, Mb was introduced to fabricate the biosensor for H_2O_2 detection. Formation and immobilization of GO@MoS_2 was confirmed by transmission electron microscopy, ultraviolet-visible spectroscopy, scanning electron microscopy, and scanning tunneling microscopy. Immobilization of Mb, and electrochemical property of biosensor were investigated by cyclic voltammetry and amperometric i-t measurements. Fabricated biosensor showed the electrochemical signal enhanced redox current as −1.86 μA at an oxidation potential and 1.95 μA at a reduction potential that were enhanced relative to those of electrode prepared without GO@MoS_2. Also, this biosensor showed the reproducibility of electrochemical signal, and retained the property until 9 days from fabrication. Upon addition of H_2O_2, the biosensor showed enhanced amperometric response current with selectivity relative to that of the biosensor prepared without GO@MoS_2. This novel hybrid material-based biosensor can suggest a milestone in the development of a highly sensitive detecting platform for biosensor fabrication with highly sensitive detection of target molecules other than H_2O_2.

1. Introduction

Nanomaterials have been of much interest and have been used in various industries, from the silicon industry to the biotechnology industry, because of their remarkable physical and chemical properties such as high strength, excellent chemical reaction rate due to their large surface area, and unique electrical properties (Hubbell and Chilkoti, 2012; Ahn et al., 2006).

Among nanomaterials, carbon nanotubes and the graphene have been widely studied by various research groups (Chae and Lee, 2014; Feng and Liu, 2011; Harrison and Atala, 2007). These carbon-based nanomaterials have unique properties, including exceptional conductivity, high electron-transfer rate, flexibility, and biocompatibility, which can be combined with biomolecules in the development bioelectronic devices and biosensors (Meyyappan, 2015).

Some research groups have found materials with properties that can surpass those of graphene. Among the potential replacements for graphene, metal dichalcogenides such as molybdenum disulfide (MoS_2), bismuth selenide (Bi_2Se_3), and indium selenide (In_2Se_3) are of interest because of their unique properties, including semiconducting property, direct band gap, conductance, and optical properties, which have diverse applications in bioelectronics (Ross et al., 2013; Chhowalla et al., 2013; Radisavljevic et al., 2011). These materials are a powerful alternative to graphene and are superior to graphene materials (Butler et al., 2013). Most studies on metal dichalcogenides have been done by using sheets of the material (Li et al., 2014a, 2014b; Ganatra and Zhang, 2014). If a nanoparticle of metal dichalcogenide is introduced for biosensor and bioelectronic application, there may be the efficient effect by extension of the activated surface area and the efficient electron transfer reaction. Graphene and metal dichalcogenides encapsulated with graphene can improve efficiency by preserving the effective carrier mobility of graphene while facilitating electron transfer at the interface (Kailashiya et al., 2015; Roy et al., 2013; Zuo et al., 2010).

Amplifying the electrochemical signal and increasing the sensitivity of biosensor used in detecting target materials is essential to measure-

* Corresponding authors at: Department of Chemical & Biomolecular Engineering, Sogang University, 35 Baekbeom-Ro, Mapo-Gu, Seoul 121-742, South Korea
E-mail addresses: jwchoi@sogang.ac.kr, bkoh@sogang.ac.kr (J.-W. Choi).

http://dx.doi.org/10.1016/j.bios.2016.11.064
Received 11 November 2016; Accepted 28 November 2016

ment of trace amounts of target molecules and thus, to commercialization of biosensors. Over the past decades, the development of biosensors based on biomolecules has been of much interest because of their application in the medical fields (Perumal and Hashim, 2014; Shu et al., 2007). Biomolecules such as DNA and proteins lead to high selectivity and a short response time (Liu et al., 2015; Zhao et al., 2014; Lee et al., 2011; Gilardi et al., 2001). In particular, the direct redox property of metalloproteins is suitable for the fast detection of specific molecules. An electrochemical signal from the metalloprotein is simply obtained by using electrochemical techniques (Lee et al., 2010, 2009; Gilardi and Fantuzzi, 2001). Choi's group developed various metalloprotein-based biosensors (Yagati et al., 2012, 2013).

However, the interaction between the metalloprotein and target molecule on a conventional electrode is met with limitations such as the unintended orientation of biomolecules on the electrode, low electrochemical signal derived from biomolecules, and slow, varying electron-transfer rate (Thudi et al., 2012; Kim et al., 2010). To overcome these, materials such as gold nanoparticles and new types of electrodes such as those based on dendritic polymers have been used to develop bioelectronic devices and biosensors with amplified electrochemical signal and sensitivity (Li et al., 2014a, 2014b; Jiménez et al., 2014; Cai et al., 2003). Graphene oxide (GO) also facilitates electron transfer from metalloproteins (Zuo et al., 2010). However, the aforementioned studies involve a complex fabrication process or have limited capacity to improve sensitivity.

Myoglobin (Mb) is a metalloprotein with unique redox properties due to the iron ion in its core. Mb can be used to detect hydrogen peroxide (H_2O_2) through electrochemical reduction of H_2O_2·H_2O_2 plays an important role in various fields, including cellular mechanisms and clinical studies (Eich et al., 1996; Wang et al., 1993)·H_2O_2 is a reactive oxygen species that affects cellular mechanisms and induces oxidative damage, which results in cell death (Panieri et al., 2013). Thus, H_2O_2 is considered a target molecule for biosensor development (Rapson et al., 2014; Zhao et al., 2005; Hedges et al., 2004).

In the present study, MoS_2 nanoparticles (MoS_2 NP) and GO were used to develop a biosensor with high sensitivity and selectivity. For the first time, MoS_2 NP were encapsulated with GO to extend the surface area of the electrode and thus to extend the area of immobilized Mb and enhance the electrochemical signal for detection. GO-encapsulated MoS_2 NP (GO@MoS_2) were immobilized on a gold electrode via a chemical linker. A biomolecular probe, Mb, was also immobilized on the electrode by an electrostatic bond (Fig. 1). Synthesis of MoS_2 NP was confirmed by transmission electron microscopy (TEM) and X-ray diffraction (XRD). Fabrication of GO@MoS_2 was confirmed by TEM and ultraviolet-visible (UV–vis) spectroscopy. Immobilization of GO@MoS_2 and Mb on the gold electrode was confirmed by scanning electron microscopy (SEM), scanning tunneling microscopy (STM), and cyclic voltammetry (CV). CV and amperometric i-t measurements were used to investigate electrochemical properties and the sensing performance of the fabricated biosensor in the detection of H_2O_2, specifically, the enhancement of electrochemical signals relative to those of the Mb-based biosensor without GO@MoS_2.

2. Experimental details

2.1. Materials

Mb (Sigma-Aldrich, USA) was prepared in phosphate-buffered saline (PBS) solution (Sigma-Aldrich, USA). A bare gold electrode composed of gold (50 nm)/Cr (2 nm)/SiO_2 was prepared by the National Nanofab Center (Korea). 6-Mercaptohexanoic acid (6-MHA) and cysteamine were purchased from Sigma-Aldrich, and H_2O_2 and H_2SO_4 were purchased from Daejung Chemical (Korea). GO was obtained from Graphene Supermarket (USA). Distilled (DI) water was purified through a Milli-Q system (Millipore, USA). Sodium molybdate, hydrazine hydrate, and Aliquat HTA-1 (Sigma-Aldrich, USA) were used as received in the synthesis of MoS_2 NP. L-Homocysteine thiolactone hydrochloride (L-hth) from Sigma-Aldrich was used in surface modification of the MoS_2 NP. TEM grids were provided by Ted Pella Inc (USA).L-Ascorbic acid (AA), sodium bicarbonate ($NaHCO_3$) and sodium nitrite ($NaNO_2$) solution (both from Sigma-Aldrich) were used to investigate the selectivity of the fabricated biosensor.

2.2. MoS_2 NP synthesis

A 4.13 mM solution of sodium molybdate (1 g) was dissolved in 25 mL of DI water in a round-bottom flask. To the resulting solution was added 2 mL of aliquat HTA-1 (1.98 g) and 40 mL of 8.24 mM of sodium sulfide solution in DI water. The reaction was allowed to proceed under a N_2 atmosphere for half an hour. A solution of 2 mL of hydrazine in 20 mL of DI water was added with constant stirring to adjust the pH to 9–10. The pH was then adjusted to 6.5 by using 0.1 mol of HCl. The solution was then heated and kept at 373 K for 4–5 h. The resulting yellowish red precipitate was filtered and thoroughly washed with DI water and alcohol. The final product, MoS_2 NP, were dried under vacuum at 70 °C for 4 h. The MoS_2 NP were characterized by high-resolution TEM using a JEOL JEM-3010 operated at 300 kV and by XRD (MiniFlex, Japan).

2.3. Encapsulation of MoS_2 NP by GO

To encapsulate MoS_2 NP with GO, the surface of MoS_2 NP was modified to disperse them. Surface modification was performed with the amine group by introducing L-hth into the MoS_2 NP. A solution of the resulting MoS_2 NP (0.1 mg/mL) was incubated with the same amount of 1 mg/mL L-hth solution for 6 h at 4 °C. L-hth was immobilized on the surface of the MoS_2 NP through a surface-chelating reaction with MoS_2 NP (Osim et al., 2013). Amine-modified MoS_2 NP were then conjugated with the same amount of 0.1 mg/mL GO solution for 6 h at 4 °C. MoS_2 NP were encapsulated with GO by electrostatic interaction to form GO@MoS_2. Fabricated GO@MoS_2 was characterized by TEM and UV–vis spectroscopy. A UV–vis spectrophotometer (Nanodrop 2000, Thermo scientific) was used to obtain UV–vis spectra.

2.4. Immobilization of GO@MoS_2 and Mb on the gold electrode

To immobilize Mb and GO@MoS_2 on the gold electrode, the electrode was treated with piranha solution (H_2SO_4/H_2O_2 solution, 8:2 vol ratio) for 3 min at 70 °C to clean the surface and to remove organic materials from the surface. Cysteamine solution (10 mM) in DI water was immobilized on the gold electrode by self-assembly for 3 h at 4 °C. GO@MoS_2 was immobilized on the gold electrode for 3 h at 4 °C by utilizing the electrostatic bond between the amine group of cysteamine and the carboxyl group of GO@MoS_2. Subsequently, Mb was immobilized on the GO@MoS_2 layer for 3 h at 4 °C, and then, Mb on GO@MoS_2-modified electrode (Mb/GO@MoS_2) was fabricated. To compare electrochemical performance of the biosensor, we fabricated a similar biosensor with immobilized Mb and without GO@MoS_2, another with immobilized Mb and GO only, and another with immobilized Mb and MoS_2 NP. To prepare electrodes with immobilized Mb and without GO@MoS_2, 6-MHA was immobilized on gold electrode treated with piranha solution for 3 h at 4 °C. Mb was immobilized on the electrode for 3 h at 4 °C by utilizing the electrostatic bond between the carboxyl group of 6-MHA and the amine group of Mb. To prepare a gold electrode with immobilized Mb and GO (Mb/GO), cysteamine was immobilized on the electrode treated with piranha solution. GO and Mb were immobilized sequentially on the electrode via electrostatic bonding. Lastly, an electrode with immobilized Mb and MoS_2 NP (Mb/MoS_2 NP) was prepared by sequential immobilization of amine-modified MoS_2 NP and Mb on the gold electrode with immobilized

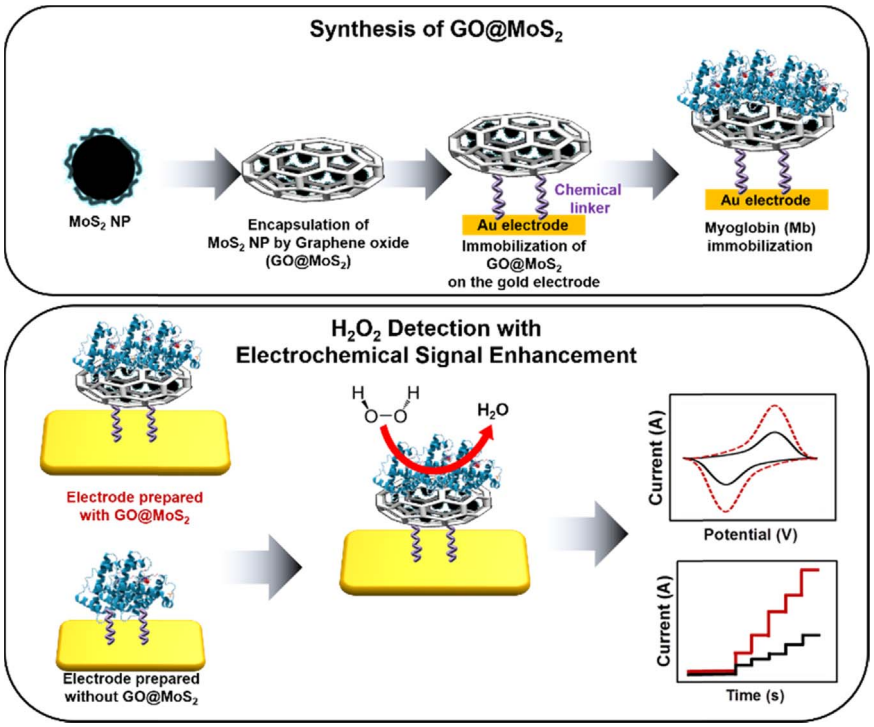

Fig. 1. Schematic of GO@MoS_2 preparation for the fabrication of electrochemical biosensors composed of Mb and of GO@MoS_2 with electrochemical enhancement for H_2O_2 detection.

6-MHA. All samples were prepared by immobilization of each components sequentially with 3 h immobilizing time due to our previous work for optimization of immobilizing time (Kim et al., 2008).

2.5. Surface investigation of GO@MoS_2 modified electrode and immobilization of Mb on the electrode

The surface morphology of gold electrode with immobilized GO@MoS_2 was investigated by STM (Nanoscope IV/Multimode (Digital Instruments, USA)). Operating parameters for STM were 0.999 Hz scan rate, 0.9 internal gain, 1.9 proportional gain, and 1.3 nA current setpoint. STM images of bare gold electrode, GO, MoS_2 NP, and GO@MoS_2 were acquired for comparison. The surface morphology of the fabricated electrode was investigated by field-emission SEM (Auriga, Carl Zeiss, Germany). Here, gold electrode with immobilized GO@MoS_2 was deposited by Pt coating. To confirm Mb immobilization on the GO@MoS_2-modified electrode, CV was performed. Unique redox peaks of Mb, which could not be acquired with the electrode without Mb immobilization, could be acquired with the electrode with immobilized Mb. Thus, immobilization of Mb on GO@MoS_2-modified electrode (Mb/GO@MoS_2) was verified by CV. Moreover, using surface profiler machine (Dektak XT, Bruker, Germany), layer formation of the proposed biosensor was further confirmed.

2.6. Investigation of electrochemical properties and sensing performance of fabricated biosensor

Electrochemical properties of the prepared biosensor were investigated through an electrochemical technique using CHI-660A (CH Instruments, Inc., USA). The setup is a three-electrode system consisting of the prepared working electrode, a silver/silver chloride (Ag/AgCl) double-junction electrode (reference electrode), and a platinum (Pt) wire electrode (counter electrode). PBS solution (pH=7.4) was used as an electrochemical buffer for the electrochemical measurements. Parameters for CV were 50 mV/s scan rate, 2 s quiet time, 1 mV/s sampling interval, and 5×10^{-7} (A/V) sensitivity. The range of applied voltage during CV was 600 mV to −200 mV. Stability and reproducibility test of the prepared biosensor were also investigated by CV. For stability test, fabricated biosensor was stored at room temperature during 9 days. Investigation of the performance in H_2O_2 detection was done through the amperometric i-t curve technique. The mechanism of electrochemical reduction of H_2O_2 may depicted as follows:

$$Mb(Fe^{3+})+e\rightarrow Mb(Fe^{2+}) \quad (1)$$

$$2Mb(Fe^{2+})+2H^{+}+H_2O_2\rightarrow 2Mb(Fe^{3+})+2H_2O \quad (2)$$

Parameters for the amperometric i-t curve were −0.3 V initial potential, 0.1 s sampling interval, and 5×10^{-7} (A/V) sensitivity.

3. Results and discussion

3.1. Confirmation of MoS_2 NP fabrication

The crystallinity and composition of the as-prepared MoS_2 NP were characterized on an XRD diffractometer using Cu Kα radiation at a scanning rate of 50/ min and within a 2Θ range of 5–90. The powder XRD pattern of the MoS_2 NP (Fig. 2a) shows broad peaks at 2Θ values of 14, 16, 24, 42, and 59, which correspond to the hexagonal phase of MoS_2 NP. The patterns also show a broad peak at 2Θ values of 42–45, which is mainly due to the amorphous nature of MoS_2 NP. No sharp peaks are present in the XRD pattern of as-prepared MoS_2 NP, indicating its poor crystallinity. Thus, the overall spectrum is typical of amorphous MoS_2. TEM analysis was carried out to study the surface morphology of the synthesized MoS_2 NP. TEM micrographs (Fig. 2b) of synthesized MoS_2 NP reveal their morphological and nanostructural details. The MoS_2 NP have an average diameter of about 10 nm and are well dispersed, stable, and uniform in size. The TEM image also confirms the well-dispersed cubic morphology of the MoS_2 NP.

3.2. Verification of GO@MoS_2 formation

Fig. 2d–f displays the results for SEM and UV–vis spectroscopy of

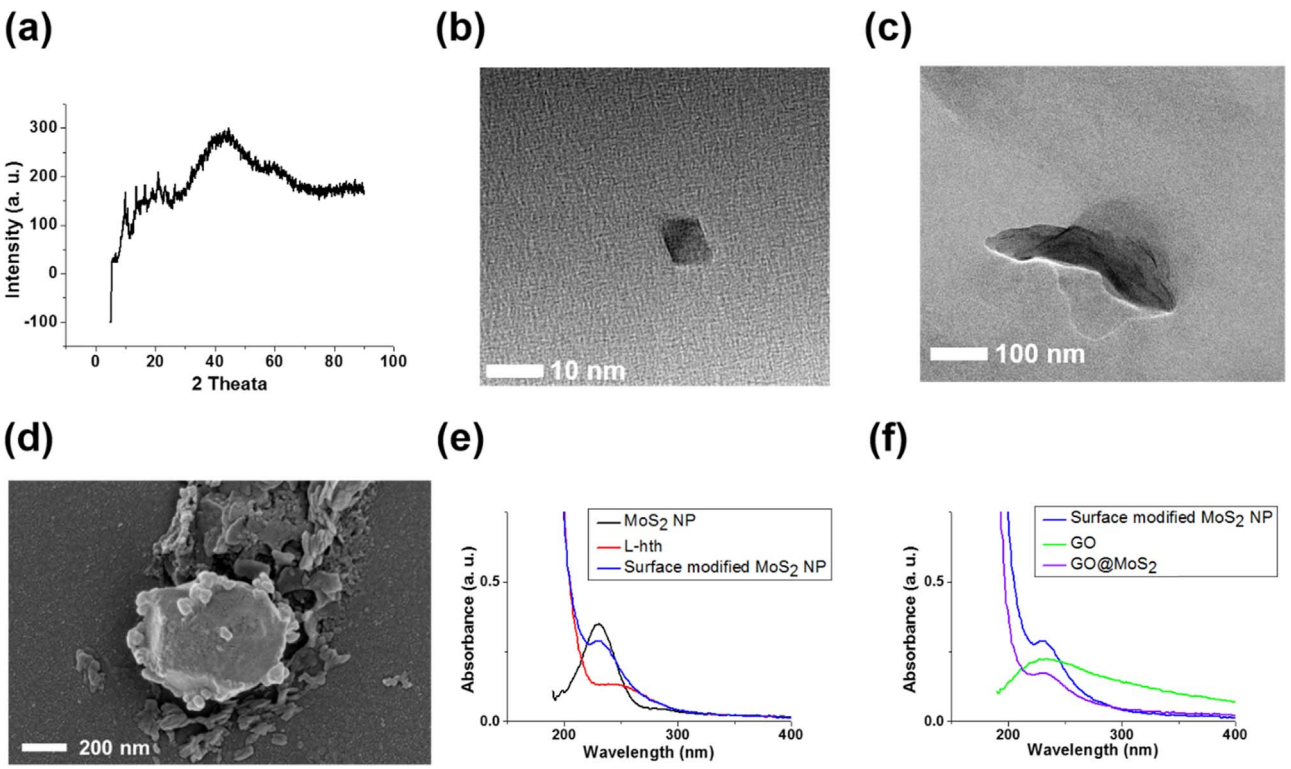

Fig. 2. (a) XRD pattern and (b) TEM images of the synthesized MoS_2 NP; (c) TEM image of GO; (d) SEM image of GO@MoS_2 immobilized on gold electrode; (e) UV–vis spectra of MoS_2 NP, L-hth, and surface-modified MoS_2 NP; (f) UV–vis spectra of surface-modified MoS_2 NP, GO, and GO@MoS_2.

GO@MoS_2, while Fig. 2c shows a TEM image of GO. The particle size of GO ranges from 200 nm to over 500 nm (not shown in Fig. 2). The aggregated form of GO was also detected. Fig. 2d presents an SEM image of GO@MoS_2 on the gold electrode. In the image, MoS_2 NP (about 10 nm in size) were encapsulated with GO (200 to >500 nm size; Fig. 2c). TEM analysis of GO@MoS_2 was also performed (Fig. S3a). In addition to SEM analysis, UV–vis spectroscopy was performed to verify the formation of GO@MoS_2. Fig. 2e and f show results of UV–vis spectroscopy. Fig. 2e shows UV spectra of MoS_2 NP, L-hth, and L-hth-modified MoS_2 NP. The UV peak for MoS_2 NP is located at 240 nm. Small and large UV peaks for L-hth are at ~250 and 220 nm, respectively. The UV result for MoS_2 NP surface-modified with L-hth shows a 240 nm peak and a large peak at 220 nm, which correspond to MoS_2 NP and L-hth, respectively. In Fig. 2f, UV peaks of surface-modified MoS_2 NP, GO, and GO@MoS_2 are shown. The UV result for GO indicates only a 230 nm peak. UV peaks for GO@MoS_2 similar to but shifted relative to those of surface-modified MoS_2 NP could be detected. They overlap with the UV peak of surface-modified MoS_2 NP at around 290 nm. At 290 nm, the UV peak of GO@MoS_2 is at a location higher than that of surface-modified MoS_2. These results may be attributed to the encapsulation of MoS_2 surface-modified by GO. Because the UV peak value of the GO is longer than that of the surface-modified MoS_2 NP by >250 nm, encapsulation of MoS_2 NP by GO resulted in a UV peak with the shape of the UV peak of GO@MoS_2.

3.3. Confirmation of GO@MoS_2 and Mb immobilization on the gold electrode

Immobilization of GO@MoS_2 on the gold electrode was verified by STM investigation and energy-dispersive X-ray spectroscopy (EDS) analysis. Mb immobilization on GO@MoS_2-modified gold electrode was confirmed by CV. Fig. 3 shows results of the STM analysis. STM images of bare gold electrode, as well as MoS_2 NP, GO, and GO@MoS_2 immobilized on electrodes, are provided in Fig. 3a–d and S1. The STM image of the bare gold electrode (Fig. 3a) reveals a regular pattern 2.98 nm in height. The STM result of MoS_2 NP immobilized on the gold electrode shows particles with sizes of around 10 nm and height of 7.95 nm (Fig. 3b). In Fig. 3c, GO particles immobilized on the gold electrode have a diameter of around 250 nm and a height of 11.75 nm. The STM image shows GO@MoS_2 particles of around 200 nm diameter and 20.82 nm height. Comparison of Fig. 3c and d reveals that GO@MoS_2 had smaller diameter and greater height compared to GO because of encapsulation of MoS_2 NP by GO. EDS data shows the composition ratio of the fabricated electrode (Fig. S2): it consisted of 40.72% carbon, 9.05% sulfur, 1.58% of molybdenum, and 48.66% of the other components silicon, gold, and chlorine, which are from both the electrode and chemical linker. Fabrication of GO@MoS_2-modified gold electrode is also confirmed by results in Fig. 3a–d. Immobilization of Mb on GO@MoS_2-modified gold electrode was confirmed by CV (Fig. S3b). The cyclic voltammogram of the GO@MoS_2-modified gold electrode has no redox peak, whereas that of GO@MoS_2-modified gold electrode with immobilized Mb apparently has a redox peak at around 0.2 V due to the redox property of Mb, thus confirming the immobilization of Mb. Also, surface profiler data showed the alteration of roughness by layer formation (Fig. S4). Roughness profile values of bare gold electrode, cysteamine-immobilized electrode, GO@MoS_2-modified electrode and Mb/GO@MoS_2 were altered by additional layer formation as shown in Fig. S4a–c of Supplementary materials. Both roughness profiles calculated by absolute values (Ra) and root mean squared (Rq) showed the increased roughness by layer formation of cysteamine, GO@MoS_2 and Mb, sequentially.

3.4. Electrochemical property of fabricated biosensor

CV was performed to investigate the redox properties of bare gold, as well as Mb, Mb/GO, Mb/MoS_2 NP, and Mb/GO@MoS_2. Fig. 4 shows cyclic voltammograms of the fabricated samples. The cyclic voltammogram of Mb/GO@MoS_2 was compared against those of the bare gold electrode and of Mb to confirm the electrochemical signal enhancement (Fig. 4a).

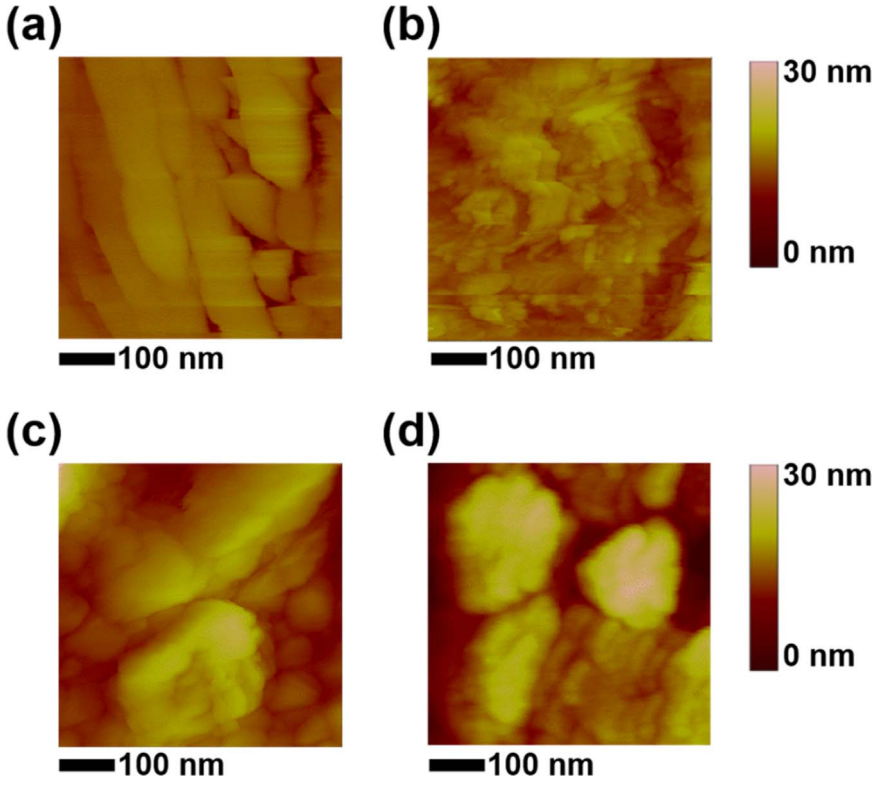

Fig. 3. STM images of (a) bare gold, (b) MoS_2 NP, (c) GO, and (d) GO@MoS_2.

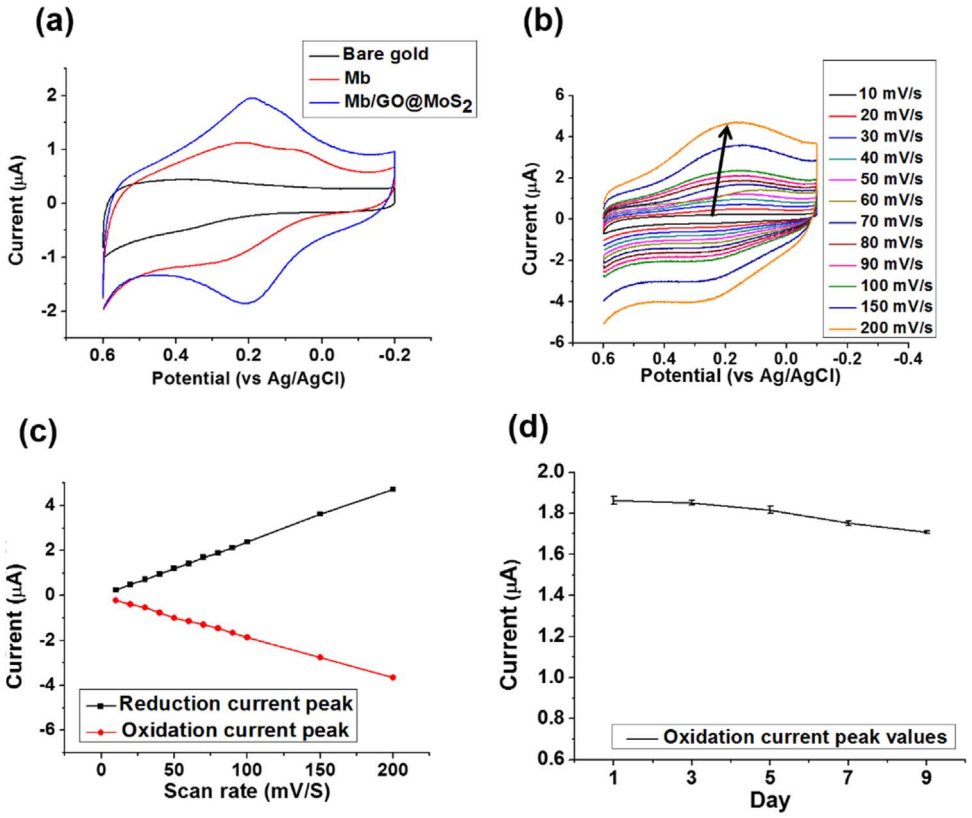

Fig. 4. (a) Cyclic voltammograms of bare gold, Mb, and Mb/GO@MoS_2; (b) cyclic voltammogram of Mb/GO@MoS_2 at scan rates increasing from 10 to 200 mV/s; (c) linear-response plot of redox current peaks of Mb/GO@MoS_2 against scan rates; (d) Stability of Mb/GO@MoS_2 at room temperature during 9 days. Error bars show the standard deviation (SD) of five measurements.

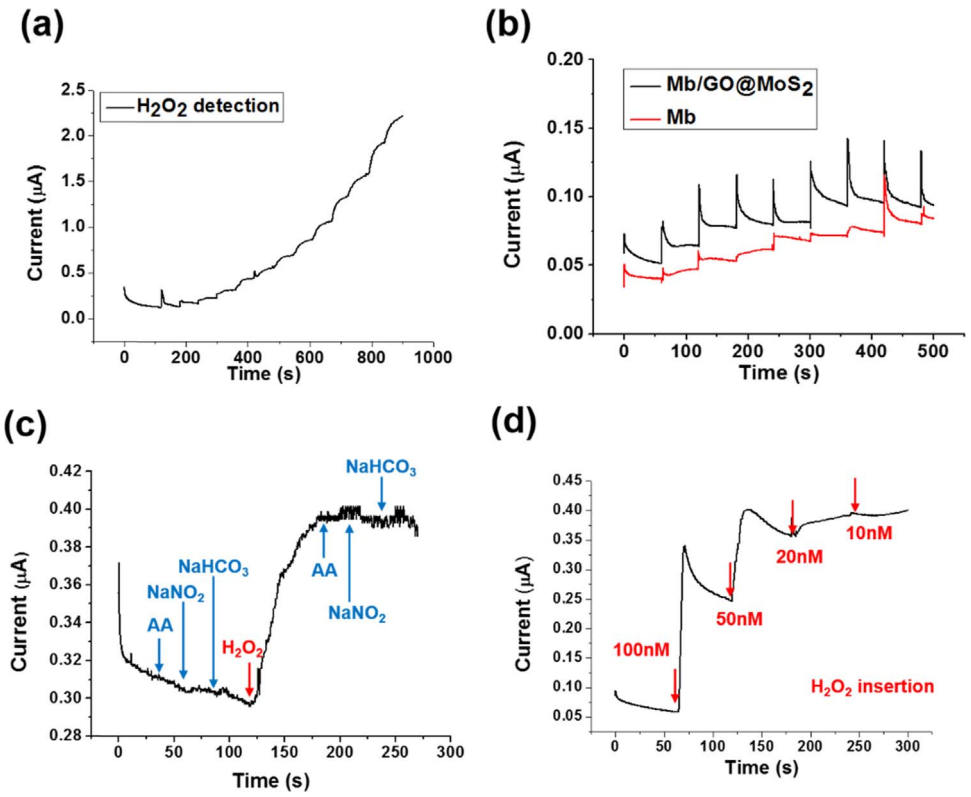

Fig. 5. Amperometric response curves of (a) Mb/GO@MoS_2 obtained by addition of 100 nM H_2O_2 solution; (b) Mb/GO@MoS_2 and Mb obtained by addition of 100 nM H_2O_2 solution; (c) Mb/GO@MoS_2 obtained upon successive addition of 100 nM L-ascorbic acid (AA), 100 nM sodium nitrite ($NaNO_2$), 100 nM sodium bicarbonate ($NaHCO_3$), and 100 nM H_2O_2 solutions; and (d) Mb/GO@MoS_2 obtained by addition of 100, 50, 20, and 10 nM H_2O_2 solutions.

The cyclic voltammogram of Mb/GO@MoS_2 shows electrochemical signal enhancement with reduction and oxidation currents of 1.95 and −1.86 μA, respectively. Those of Mb are 1.12 and −1.04 μA, respectively, which are lower than those of Mb/GO@MoS_2. The cyclic voltammogram of Mb/GO@MoS_2 shows enhancement of electrochemical signals relative to those of Mb/GO and Mb/MoS_2 NP (Fig. S5a and b). Signal enhancement with Mb/GO@MoS_2 may be attributed to facilitation of electron-transfer reaction between the gold electrode and Mb by localization of GO@MoS_2 between the electrode and Mb. It may also be due to extension of the surface area for Mb immobilization due to immobilization of GO@MoS_2 on the gold electrode. Also, this fabricated electrode showed the reproducibility with 1.94 μA at reduction peak current and −1.86 μA at oxidation peak current averagely (Fig. S5c). Average values and error bars were acquired by standard deviation (SD) of five measurements. The cyclic voltammogram of Mb/GO@MoS_2 (Fig. 4b) was acquired by increasing scan rates from 10 mV/s to 200 mV/s. With increasing scan rates, both redox peaks of Mb/GO@MoS_2 slightly shifted to the right. Redox current peaks of Mb/GO@MoS_2 are shown as a linear plot against scan rates (Fig. 4c). This prepared biosensor with Mb/GO@MoS_2 retained the redox properties until 9 days stored at room temperature with slight decrease of redox peak currents from 1.87 μA in the first day to 1.71 μA in 9 day (Fig. 4d). After 9 days from fabrication, this biosensor even showed the enhanced electrochemical redox peaks compared to the results of Mb modified electrode. Error bars in Fig. 4d shows the standard deviation (SD) of five measurements. The biocompatible property of GO may affect the stability of fabricated biosensor at room temperature for 9 days.

3.5. Amperometric response of fabricated biosensor for H_2O_2 detection

A chronoamperometric experiment using the amperometric i-t curve technique was done on Mb/GO@MoS_2 to measure the catalytic response of the biosensor. The amperometric response of the biosensor was acquired by successive addition of 10 μL of 10 mM H_2O_2 solution to 3 mL of the electrolyte, PBS solution. The initial potential −0.2 V was selected to achieve complete reduction of Mb before the catalytic response. Fig. 5 shows the amperometric response curve for the catalytic reaction of Mb/GO@MoS_2 upon addition of H_2O_2. The reduction current for the biosensor (Fig. 5a) increased steeply and reached a stable value whenever H_2O_2 was added over 10 times. Amperometric responses of Mb/GO@MoS_2 and Mb upon addition of H_2O_2 may be compared in Fig. 5b. The Mb/GO@MoS_2-modified electrode showed an enhanced electrochemical amperometric response as compared with that of the Mb immobilized electrode, quickly reaching steady state because of fast electron transfer upon introduction of GO@MoS_2. To confirm the selectivity of the fabricated biosensor, AA, $NaNO_2$ and $NaHCO_3$ were added continuously with H_2O_2. Fabricated biosensor showed the amperometric response only with injection of H_2O_2. Fig. 5c shows the selectivity of the amperometric response of the biosensor to H_2O_2. To verify the detection limit of the biosensor, different concentrations of H_2O_2 (100, 50, 20, and 10 nM) were added to the electrode (Fig. 5d). According to the amperometric results, the detection limit of the biosensor for H_2O_2 is 20 nM. The detection limit of this biosensor is more sensitive and comparable to that of other electrodes for H_2O_2 detection in terms of detection limit (Table. S1). Furthermore, this biosensor was prepared with simple fabricating process compared to the other electrodes mentioned in Table. S1.

4. Conclusions

In this study, an electrochemical biosensor composed of Mb and GO@MoS_2 with enhanced electrochemical signal was fabricated for H_2O_2 detection. GO@MoS_2 was fabricated for the first time to induce

the electrochemical signal enhancement of the biosensor. Synthesis of MoS_2 NP and fabrication of GO@MoS_2 were verified by TEM, XRD, and UV–vis spectroscopy. Preparation of the biosensor was confirmed by STM, SEM, EDS and CV. Results of electrochemical investigation suggest that the biosensor has an electrochemical signal of −1.86 μA at the oxidation potential peak and 1.95 μA at the reduction potential peak. These redox currents are much larger than those for the peaks of Mb, Mb/GO, and Mb/MoS_2 NP. Also, this biosensor showed the reproducibility and retained stable redox peak currents until 9 days at room temperature. The electrochemical amperometric response of the biosensor, the reduction current, increased relative to that for Mb without GO@MoS_2 upon addition of H_2O_2 solution at 20 nM concentration level. This biosensor also showed selective detection of H_2O_2 in mixtures injected with AA, $NaNO_2$ and $NaHCO_3$. By introduction of hybrid material composed of GO@MoS_2 to prepare biosensor for the first time, GO@MoS_2 affected the fast electron transfer and surface extension with biocompatibility to enhance the electrochemical signal and amperometric response. Still, further study related to GO@MoS_2 for the development of biosensor should be needed to apply *in vivo* or real sample detection. Nevertheless, the proposed GO@MoS_2 modified electrode can suggest a milestone in the development of a highly sensitive detecting platform for biosensor fabrication.

Acknowledgement

This research was supported by the Leading Foreign Research Institute Recruitment Program, through the National Research Foundation of Korea (NRF), funded by the Ministry of Science, ICT and Future Planning (MSIP) (2013K1A4A3055268) and by the National Research Foundation of Korea (NRF) grant funded by the Korea Government (MSIP) (no. 2014R1A2A1A10051725) and Basic Science Research Program through the National Research Foundation of Korea (NRF) funded by the Ministry of Education (2016R1A6A1A03012845).

Appendix A. Supplementary material

Supplementary material associated with this article can be found in the online version at doi:10.1016/j.bios.2016.11.064.

References

Ahn, J.-H., Kim, H.-S., Lee, K.J., Jeon, S., Kang, S.J., Sun, Y., Nuzzo, R.G., Rogers, J.A., 2006. Science 314, 1754–1757.
Butler, S.Z., Hollen, S.M., Cao, L., Cui, Y., Gupta, J.A., Gutiérrez, H.R., Heinz, T.F., Hong, S.S., Huang, J., Ismach, A.F., Johnston-Halperin, E., Kuno, M., Plashnitsa, V.V., Robinson, R.D., Ruoff, R.S., Salahuddin, S., Shan, J., Shi, L., Spencer, M.G., Terrones, M., Windl, W., Goldberger, J.E., 2013. ACS Nano 7, 2898–2926.
Cai, H., Cao, X., Jiang, Y., He, P., Fang, Y., 2003. Anal. Bioanal. Chem. 375, 287–293.
Chae, S.H., Lee, Y.H., 2014. Nano Converg. 1, 15.
Chhowalla, M., Shin, H.S., Eda, G., Li, L.-J., Loh, K.P., Zhang, H., 2013. Nat. Chem. 5, 263–275.
Eich, R.F., Li, T., Lemon, D.D., Doherty, D.H., Curry, S.R., Aitken, J.F., Mathews, A.J., Johnson, K.A., Smith, R.D., Phillips, G.N., Jr, Olson, J.S., 1996. Biochemistry 35, 6976–6983.
Feng, L., Liu, Z., 2011. Nanomedicine 6, 317–324.
Ganatra, R., Zhang, Q., 2014. ACS Nano 8, 4074–4099.
Gilardi, G., Fantuzzi, A., 2001. Trends Biotechnol. 19, 468–476.
Gilardi, G., Fantuzzi, A., Sadeghi, S.J., 2001. Curr. Opin. Struct. Biol. 11, 491–499.
Harrison, B.S., Atala, A., 2007. Biomaterials 28, 344–353.
Hedges, D.H.P., Richardson, D.J., Russell, D.A., 2004. Langmuir 20, 1901–1908.
Hubbell, J.A., Chilkoti, A., 2012. Science 337, 303–305.
Jiménez, A., Armada, M.P.G., Losada, J., Villena, C., Alonso, B., Casado, C.M., 2014. Sens. Actuator B-Chem. 190, 111–119.
Kailashiya, J., Singh, N., Singh, S.K., Agrawal, V., Dash, D., 2015. Biosens. Bioelectron. 65, 274–280.
Kim, S.-U., Kim, Y.J., Choi, S.-G., Yea, C.-H., Singh, R.P., Min, J., Oh, B.-K., Choi, J.-W., 2008. Ultramicroscopy 108, 1390–1395.
Kim, S.-U., Yagati, A.K., Min, J., Choi, J.-W., 2010. Biomaterials 31, 1293–1298.
Lee, K.-P., Gopalan, A.L., Komathi, S., 2009. Sens. Actuator B-Chem. 141, 518–525.
Lee, T., Kim, S.-U., Min, J., Choi, J.-W., 2010. Adv. Mater. 22, 510–514.
Lee, T., Yoo, S.-Y., Chung, Y.-H., Min, J., Choi, J.-W., 2011. Electroanal 23, 2023–2029.
Li, H., Wu, J., Yin, Z., Zhang, H., 2014a. Acc. Chem. Res. 47, 1067–1075.
Li, K., Liu, G., Wu, Y., Hao, P., Zhou, W., Zhang, Z., 2014b. Talanta 120, 419–424.
Liu, J., Wang, T., Wang, J., Wang, E., 2015. Electrochim. Acta 161, 17–22.
Meyyappan, M., 2015. Nano Converg. 2, 18.
Osim, W., Stojanovic, A., Akbarzadeh, J., Peterlik, H., Binder, W.H., 2013. Chem. Commun. 49, 9311–9313.
Panieri, E., Gogvadze, V., Norberg, E., Venkatesh, R., Orrenius, S., Zhivotovsky, B., 2013. Free Radic. Biol. Med. 57, 176–187.
Perumal, V., Hashim, U., 2014. J. Appl. Biomed. 12, 1–15.
Radisavljevic, B., Radenovic, A., Brivio, J., Giacometti, V., Kis, A., 2011. Nat. Nanotechnol. 6, 147–150.
Rapson, T.D., Church, J.S., Trueman, H.E., Dacres, H., Sutherland, T.D., Trowell, S.C., 2014. Biosens. Bioelectron. 62, 214–220.
Ross, J.S., Wu, S., Yu, H., Ghimire, N.J., Jones, A.M., Aivazian, G., Yan, J., Mandrus, D.G., Xiao, D., Yao, W., Xu, X., 2013. Nat. Commun. 4, 1474.
Roy, K., Padmanabhan, M., Goswami, S., Sai, T.P., Ramalingam, G., Raghavan, S., Ghosh, A., 2013. Nat. Nanotechnol. 8, 826–830.
Shu, X., Chen, Y., Yuan, H., Gao, S., Xiao, D., 2007. Anal. Chem. 79, 3695–3702.
Thudi, L., Jasti, L.S., Swarnalatha, Y., Fadnavis, N.W., Mulani, K., Deokar, S., Ponrathnam, S., 2012. Colloids Surf. B 90, 184–190.
Wang, J., Lin, Y., Chen, L., 1993. Analyst 118, 277–280.
Yagati, A.K., Lee, T., Min, J., Choi, J.-W., 2012. Colloids Surf. B 92, 161–167.
Yagati, A.K., Lee, T., Min, J., Choi, J.-W., 2013. Biosens. Bioelectron. 47, 385–390.
Zhao, G.-C., Yin, Z.-Z., Zhang, L., Wei, X.-W., 2005. Electrochem. Commun. 7, 256–260.
Zhao, W. –W., Xu, J. –J., Chen, H. –Y., 2014. Chem. Rev. 114, 7421–7441.
Zuo, X., He, S., Li, D., Peng, C., Huang, Q., Song, S., Fan, C., 2010. Langmuir 26, 1936–1939.